

Protection of all nondefective twofold degeneracies by anti-unitary symmetries in non-Hermitian systems

Sharareh Sayyad^{1, *}

¹*Max Planck Institute for the Science of Light, Staudtstraße 2, 91058 Erlangen, Germany*
(Dated: December 23, 2022)

Non-Hermitian degeneracies are classified as defective exceptional points (EPs) and nondefective degeneracies. While in defective EPs, both eigenvalues and eigenvectors coalesce, nondefective degeneracies are characterized merely by the emergence of degenerate eigenvalues. It is also known that all degeneracies are either symmetry-protected or accidental. In this paper, I prove that anti-unitary symmetries protect all nondefective twofold degeneracies. By developing a 2D non-Hermitian tight-binding model, I have demonstrated that these symmetries comprise various symmetry operations, such as discrete or spatial point-group symmetries and Wick's rotation in the non-Hermitian parameter space. Introducing these composite symmetries, I present the protection of nondefective degeneracies in various parameter regimes of my model. This work paves the way to stabilizing nondefective degeneracies and offers a new perspective on understanding non-Hermitian band crossings.

Introduction.— Appearance of degeneracies in the energy spectra of different Hermitian systems gives rise to a plethora of phenomena such as quantized classical [1–3] and quantum [4–9] responses, quantum anomalies [10–14] and the emergence of novel effective quasiparticles [15–20]. The occurrence of degenerate energy levels historically has been classified into either symmetry-protected or accidental degeneracies [21–25]. Here, accidental degeneracies refer to the intersection of energy levels due to the fine-tuning of parameters without symmetry stabilization. It has been later discussed that all band-touching points in two-band Hermitian systems are protected by anti-unitary symmetries dubbed “hidden symmetries” [26–29]. Accidental degeneracies are stable in these systems as long as these hidden symmetries are respected. It has further been shown that these hidden symmetries are usually composite of various discrete operations, including rotation, translation, sublattice exchange, and complex conjugation.

Another platform where degeneracies play a crucial role is in non-Hermitian physics, which effectively describes open systems. This field of study encounters surges of interest as some of its underlying properties have no Hermitian counterparts [30–32]. The appearance of defective exceptional points (EPs) [33, 34], at which both eigenvalues and eigenvectors coalesce, and the accumulation of bulk modes on the boundaries, known as the skin effect [35–40], exemplify prominent properties of non-Hermitian systems which cannot be realized in Hermitian setups. Aside from these possibilities, non-Hermitian systems may accommodate other degeneracies which are nondefective [41–45]. These nondefective degeneracies can be further classified into two classes. While one type of these nondefective degeneracies has an analog in Hermitian physics and is usually isolated [46], the other type resides in the vicinity of defective EPs [47] and hence has no counterparts in Hermitian physics [44]. All of these non-Hermitian degen-

eracies, as well as the skin effect in non-Hermitian systems, is under theoretical investigation and experimental observation in various field of research, including classical active matters [48, 49], classical electric circuits [50–53], quantum circuits [54], photonics [55–59], phononics [60, 61], laser physics [62–64], field theories [65–67], transport physics [68–71] and non-equilibrium dynamics [72–74].

The spate of studies on EPs identifies numerous (spatial or discrete) symmetries which protect defective EPs [44, 75–80]. It has also been shown that the intersection of an even number of symmetry-protected higher-dimensional defective EPs, e.g., exceptional rings, results in observing nondefective degeneracies [44, 80, 81]. Hence, all nondefective degeneracies found in these situations are also stabilized by symmetry, which protects the defective EPs [75, 77, 82]. Further attempt regarding symmetry stabilization of isolated nondefective degeneracies is based on a case study on four-band models and in the presence of two symmetries, namely pseudo-Hermiticity and anti-parity-time symmetries, which impose strict restrictions on the eigenspace of the model [42]. However, the analog between well-studied Hermitian degeneracies and nondefective degeneracies urges one to go beyond the case studies and identify the key factors that make any nondefective degeneracies robust.

As I have pointed out, all accidental degeneracies in two-band Hermitian systems are symmetry protected. One may wonder whether the stabilization of Hermitian accidental degeneracies can be extended to the realm of non-Hermitian physics. In this Letter, I prove that composite anti-unitary symmetries protect all twofold nondefective degeneracies in non-Hermitian models. I further demonstrate that, due to the biorthogonality of the eigenspace, these symmetry operators come in (right and left) pairs. By introducing a 2D non-Hermitian tight-binding model, I show that different non-Hermitian com-

posite symmetries protect nondefective degeneracies in various parameter regimes in my model. These composite symmetries are distinct from their Hermitian counterparts due to the presence of a Wick's rotation in the non-Hermitian parameter regime.

Theorem.— In the following, I prove that *all non-defective twofold degeneracies in non-Hermitian systems are protected by anti-unitary operations with nonunity square.*

The eigensystem of a two-band non-Hermitian Hamiltonian \mathcal{H}_{nH} with nondefective degeneracy ($\lambda = \lambda_0$) casts

$$\mathcal{H}_{\text{nH}}|\psi_i^R\rangle = \lambda_0|\psi_i^R\rangle, \quad \langle\psi_i^L|\mathcal{H}_{\text{nH}} = \langle\psi_i^L|\lambda_0, \quad (1)$$

$$\mathcal{H}_{\text{nH}}^\dagger|\psi_i^L\rangle = \lambda_0^*|\psi_i^L\rangle, \quad \langle\psi_i^R|\mathcal{H}_{\text{nH}}^\dagger = \langle\psi_i^R|\lambda_0^*. \quad (2)$$

where $|\psi_i^{R/L}\rangle$ with $i \in \{1, 2\}$ denotes the right/left biorthogonal eigenvector such that $\langle\psi_j^L|\psi_i^R\rangle = \delta_{ij}$.

In Hermitian systems, the Hermiticity imposes that vanishing the commutation relation between the symmetry operator and the Hamiltonian leads to the invariance of the system under a particular symmetry. However, due to the lack of Hermiticity in non-Hermitian models, biorthogonality of eigenvectors necessitates introducing left and right symmetry operations such that, see also the Supplemental Material (SM) [83],

$$\mathcal{H}_{\text{nH}}^\dagger \Upsilon_{\text{nH}}^R - \Upsilon_{\text{nH}}^R \mathcal{H}_{\text{nH}} = 0, \quad (3)$$

$$\mathcal{H}_{\text{nH}} \Upsilon_{\text{nH}}^L - \Upsilon_{\text{nH}}^L \mathcal{H}_{\text{nH}}^\dagger = 0. \quad (4)$$

The explicit form of these symmetry operators in terms of biorthogonal basis reads [84]

$$\Upsilon_{\text{nH}}^R = [|\psi_1^R\rangle\langle\psi_2^{R*}| - |\psi_2^R\rangle\langle\psi_1^{R*}|] \mathcal{K}, \quad (5)$$

$$\Upsilon_{\text{nH}}^L = [|\psi_1^L\rangle\langle\psi_2^{L*}| - |\psi_2^L\rangle\langle\psi_1^{L*}|] \mathcal{K}, \quad (6)$$

where \mathcal{K} is the complex conjugation operator that ensures $\Upsilon_{\text{nH}}^{R/L}$ is anti-unitary. Employing Eqs. (5, 6), one can verify that $\Upsilon_{\text{nH}}^R \cdot \Upsilon_{\text{nH}}^L = \Upsilon_{\text{nH}}^L \cdot \Upsilon_{\text{nH}}^R = -\mathbb{1}$ [85]. Applying these symmetries on biorthogonal eigenvectors then yields

$$\Upsilon_{\text{nH}}^R|\psi_2^L\rangle = |\psi_1^R\rangle, \quad \Upsilon_{\text{nH}}^R|\psi_1^L\rangle = -|\psi_2^R\rangle, \quad (7)$$

$$\Upsilon_{\text{nH}}^L|\psi_2^R\rangle = |\psi_1^L\rangle, \quad \Upsilon_{\text{nH}}^L|\psi_1^R\rangle = -|\psi_2^L\rangle. \quad (8)$$

From Eqs. (7, 8), I realize that both eigenvectors in $(\Upsilon_{\text{nH}}^R|\psi_1^L\rangle, |\psi_1^R\rangle)$ or in $(\Upsilon_{\text{nH}}^L|\psi_1^R\rangle, |\psi_1^L\rangle)$ possess the degenerate eigenvalue λ_0 or λ_0^* , respectively.

To corroborate that these degeneracies are protected by symmetry with a nonunity square, I in the following show that eigenvectors are orthogonal by calculating the overlap of eigenvectors at the nondefective degenerate point. For an anti-unitary operator Υ in Hermitian systems, one can rewrite the overlap of eigenvectors as $\langle\psi|\phi\rangle = \langle\Upsilon\phi|\Upsilon\psi\rangle$. In non-Hermitian setups, biorthogonality of eigenvectors results in generalizing this relation

using Υ^R and Υ^L into

$$\begin{cases} \langle\psi^L|\phi^R\rangle &= \langle\Upsilon^L\phi^R|\Upsilon^R\psi^L\rangle, \\ \langle\psi^R|\phi^L\rangle &= \langle\Upsilon^R\psi^L|\Upsilon^L\phi^R\rangle. \end{cases} \quad (9)$$

Having this and by defining $\Upsilon_{\text{nH}}^L|\psi_1^R\rangle = |\tilde{\psi}_1^L\rangle$ and $\Upsilon_{\text{nH}}^R|\psi_1^L\rangle = |\tilde{\psi}_1^R\rangle$, I evaluate the inner products as

$$\begin{aligned} \langle\psi_1^L|\tilde{\psi}_1^R\rangle &= \langle\Upsilon_{\text{nH}}^L\tilde{\psi}_1^R|\Upsilon_{\text{nH}}^R\psi_1^L\rangle, \\ &= \langle\Upsilon_{\text{nH}}^L\Upsilon_{\text{nH}}^R\psi_1^L|\Upsilon_{\text{nH}}^R\psi_1^L\rangle, \\ &= -\langle\psi_1^L|\Upsilon_{\text{nH}}^R\psi_1^L\rangle, \\ &= -\langle\psi_1^L|\tilde{\psi}_1^R\rangle, \end{aligned} \quad (10)$$

$$\begin{aligned} \langle\psi_1^R|\tilde{\psi}_1^L\rangle &= \langle\Upsilon_{\text{nH}}^R\tilde{\psi}_1^L|\Upsilon_{\text{nH}}^L\psi_1^R\rangle, \\ &= \langle\Upsilon_{\text{nH}}^R\Upsilon_{\text{nH}}^L\psi_1^R|\Upsilon_{\text{nH}}^L\psi_1^R\rangle, \\ &= -\langle\psi_1^R|\Upsilon_{\text{nH}}^L\psi_1^R\rangle, \\ &= -\langle\psi_1^R|\tilde{\psi}_1^L\rangle. \end{aligned} \quad (11)$$

The above relations can be also verified using Eq. (7, 8). Here I set $\Upsilon_{\text{nH}}^R\Upsilon_{\text{nH}}^L|\psi_1^R\rangle = -|\psi_1^R\rangle$ and $\Upsilon_{\text{nH}}^L\Upsilon_{\text{nH}}^R|\psi_1^L\rangle = -|\psi_1^L\rangle$ to get the third line of the above relations. Eqs. (10, 11) does not hold unless the set of eigenvectors in $(\Upsilon_{\text{nH}}^R|\psi_1^L\rangle, |\psi_1^R\rangle)$ and in $(\Upsilon_{\text{nH}}^L|\psi_1^R\rangle, |\psi_1^L\rangle)$ are orthogonal, i.e., $\langle\psi_1^L|\psi_1^R\rangle = \langle\psi_1^R|\tilde{\psi}_1^L\rangle = 0$. Hence, I conclude that the presence of a pair of non-Hermitian anti-unitary symmetry (Υ^R, Υ^L) with $\Upsilon^R \cdot \Upsilon^L = -1$ protects nondefective degeneracies in non-Hermitian systems. ■

To exemplify our findings, I now explore the stabilization of nondefective degeneracies by non-Hermitian symmetries on a 2D square lattice.

2D Tight-binding model.— I consider a non-Hermitian bipartite model on a square lattice with staggered potentials, non-reciprocal hopping terms, and nonzero Peierls phase factors for nearest-neighbor hopping amplitudes, schematically shown in Fig. 1. Our model Hamiltonian, which is the non-Hermitian generalization of the model in Ref. [26], reads

$$\mathcal{H} = \mathcal{H}_0 + \mathcal{H}_1 + \mathcal{H}_2, \quad (12)$$

$$\begin{aligned} \mathcal{H}_0 &= -t \left[e^{-i\gamma} e^{-g_x} a_i^\dagger b_{i+\hat{x}} + e^{-i\gamma} e^{-g_x} a_i^\dagger b_{i-\hat{x}} \right. \\ &\quad + e^{i\gamma} e^{-g_y} a_i^\dagger b_{i+\hat{y}} + e^{i\gamma} e^{-g_y} a_i^\dagger b_{i-\hat{y}} \\ &\quad + e^{i\gamma} e^{g_x} b_{i+\hat{x}}^\dagger a_i + e^{i\gamma} e^{g_x} b_{i-\hat{x}}^\dagger a_i \\ &\quad \left. + e^{-i\gamma} e^{g_y} b_{i+\hat{y}}^\dagger a_i + e^{-i\gamma} e^{g_y} b_{i-\hat{y}}^\dagger a_i \right], \end{aligned} \quad (13)$$

$$\begin{aligned} \mathcal{H}_1 &= -t_1 \left[e^{-g_a} a_i^\dagger a_{i+\hat{x}+\hat{y}} - e^{-g_a} a_i^\dagger a_{i+\hat{x}-\hat{y}} \right. \\ &\quad - e^{-g_b} b_i^\dagger b_{i+\hat{x}+\hat{y}} + e^{-g_b} b_i^\dagger b_{i+\hat{x}-\hat{y}} \\ &\quad + e^{g_a} a_{i+\hat{x}+\hat{y}}^\dagger a_i - e^{g_a} a_{i+\hat{x}-\hat{y}}^\dagger a_i \\ &\quad \left. - e^{g_b} b_{i+\hat{x}+\hat{y}}^\dagger b_i + e^{g_b} b_{i+\hat{x}-\hat{y}}^\dagger b_i \right], \end{aligned} \quad (14)$$

$$\mathcal{H}_2 = v \sum_{i \in A} a_i^\dagger a_i - v \sum_{i \in B} b_i^\dagger b_i, \quad (15)$$

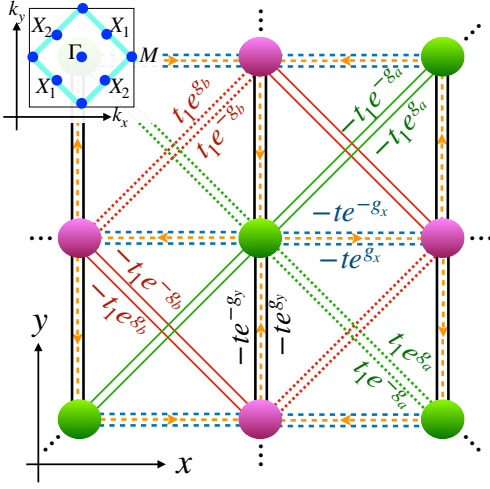


Figure 1. Illustration of the tight-binding model on the square lattice with A (green) and B (magenta) sublattices. Various nearest neighbor and next nearest neighbor hopping amplitudes are shown in solid and dashed lines. The Peierls phase along x or y directions are shown with orange dashed line arrows. The inset displays the first Brillouin zone delineated by the cyan solid line. The high symmetry points, shown in blue, are at $(k_x, k_y) = (0,0)$ at the Γ point, $(\pi, 0)$ at the M point, $\{(\pi/2, \pi/2), (-\pi/2, -\pi/2)\}$ at the X_1 points, and $\{(\pi/2, -\pi/2), (-\pi/2, \pi/2)\}$ at the X_2 points.

where $a_i^\dagger (b_i^\dagger)$ creates an electron at site i in sublattice A (B) and \hat{x} (\hat{y}) stands for unit vectors along the x (y) direction. Here t is the nearest-neighbor hopping amplitude, t_1 denotes the diagonal hopping amplitude, v sets the staggered onsite potential, γ is the Peierls phase and (g_x, g_y, g_a, g_b) account nonreciprocity.

The above quadratic Hamiltonian in the momentum space using $F^\top = (a_{\mathbf{k}}, b_{\mathbf{k}})$ casts

$$\mathcal{H}(\mathbf{k}) = F^\dagger h_{\mathbf{k}} F, \text{ with } h_{\mathbf{k}} = \begin{pmatrix} h_{11} & h_{12} \\ h_{21} & h_{22} \end{pmatrix}, \quad (16)$$

where $h_{11} = -t_1(-e^{-g_a - i(k_x - k_y)} - e^{g_a + i(k_x - k_y)} + e^{-g_a - i(k_x + k_y)} + e^{g_a + i(k_x + k_y)}) + i\mu_a + v$, $h_{22} = t_1(-e^{-g_b - i(k_x - k_y)} - e^{g_b + i(k_x - k_y)} + e^{-g_b - i(k_x + k_y)} + e^{g_b + i(k_x + k_y)}) - i\mu_b - v$, $h_{12} = -2te^{-g_x - i\gamma} \cos(k_x) - 2te^{-g_y + i\gamma} \cos(k_y)$ and $h_{21} = -2te^{g_x + i\gamma} \cos(k_x) - 2te^{g_y - i\gamma} \cos(k_y)$.

The spectrum of this Hamiltonian yields $\epsilon_{\pm} = (\text{tr}[h_{\mathbf{k}}] \pm \sqrt{\eta})/2$, with $\eta = \text{tr}[h_{\mathbf{k}}]^2 - 4\det[h_{\mathbf{k}}]$. Here, $\text{tr}[h_{\mathbf{k}}]$ and $\det[h_{\mathbf{k}}]$ denote the trace and the determinant of $h_{\mathbf{k}}$, respectively. The complex-valued η is the discriminant of the characteristic polynomial. The solutions of $\eta = 0$ are degeneracies of $h_{\mathbf{k}}$ [31, 78].

Our model Hamiltonian accommodates various quantum phases, including the linear Weyl and quadratic double-Weyl semimetals as well as the trivial and topological band insulators; see the SM for details [83]. In the following, I focus on exploring various parameter regimes

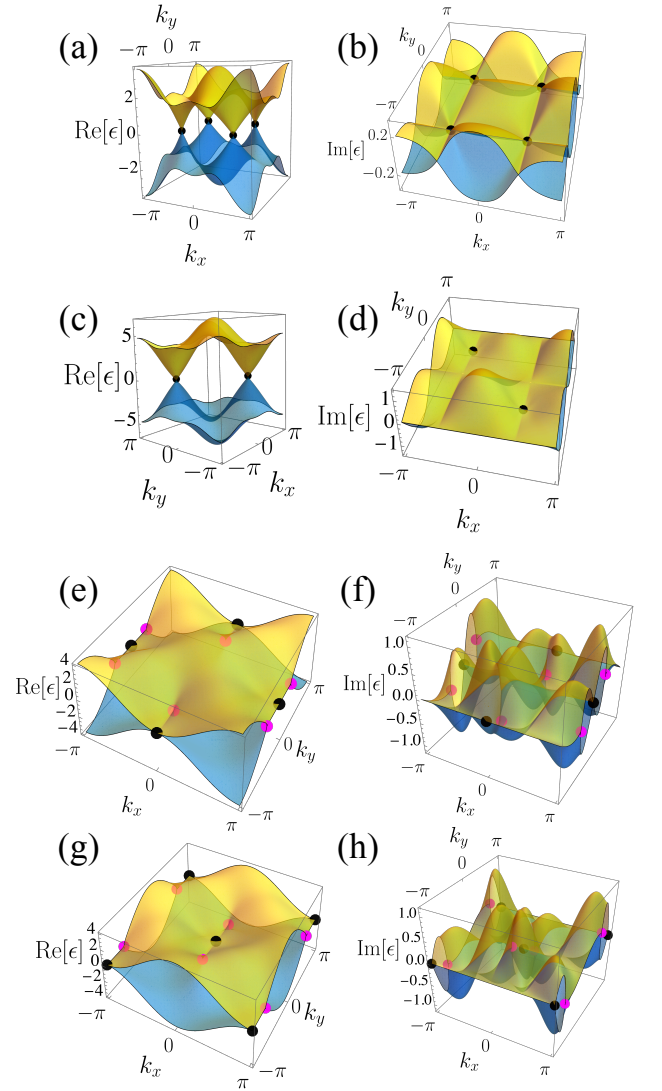


Figure 2. Real (left panels) and imaginary (right) parts of the energy dispersion at various parameter regimes. For each panel, I set $(\gamma, g_x, g_y, t_1/t, g_a, g_b, v/t) = (0.5, 0.5, 0.3, 0.0, 0.0, 0.0, 0.0)$ (a,b), $(0.5, 0.0, 0.0, 0.75, 0.5, 0.3, 3.26)$ (c,d), $(0.0, 0.0, 0.0, 0.75, 0.5, 0.3, 0.0)$ (e,f), $(\pi/2, 0.0, 0.0, 0.75, 0.5, 0.3, 0.0)$ (g,h). Magenta points mark the defective EPs, and black points indicate nondefective degeneracies. Line colors are chosen such that the largest (smallest) values are presented in yellow (blue).

within which nondefective degeneracies find room to emerge.

nondefective degeneracies at $t_1 = g_a = g_b = v = 0$.— The first parameter regime in which nondefective degeneracies arise is at $t_1 = g_a = g_b = v = 0$. Here the model Hamiltonian merely comprises nearest-neighbor hopping terms, i.e., $\mathcal{H} = \mathcal{H}_0$; see the SM [83]. Setting $0 < \gamma < \pi/2$ in \mathcal{H} leads to observing nondefective degeneracies in the band structure of our system. Fig. 2 depicts the real (a) and imaginary (b) parts of the spec-

trum at $\gamma = 0.5$, $g_x = 0.5$ and $g_y = 0.3$. The nondefective degeneracies, indicated by black points, appear at the X points at $(k_x, k_y) = (\pm\pi/2, \pm\pi/2)$ shown in the inset of Fig. 1 when $\cos(k_x) = \cos(k_y) = 0$.

The composite symmetry, which guarantees the occurrence of nondefective degeneracies, reads $\Upsilon_R = \sigma_x \mathcal{K} \mathcal{W}_g \mathcal{T}_{\hat{x}}$ and $\Upsilon_L = \sigma_x \mathcal{K} \mathcal{W}_{-g} \mathcal{T}_{\hat{x}}$ with $\Upsilon_R \cdot \Upsilon_L = \mathcal{T}_{2\hat{x}}$. Here $\mathcal{T}_{\hat{x}}$ is the translational symmetry along the x axis, and \mathcal{W}_g imposes the Wick's rotation on g_x and g_y such that $\mathcal{W}_g g_{x/y} \mathcal{W}_g^{-1} = i g_{x/y}$ [86]. I note that $\mathcal{K} \mathcal{W}_g$ is equivalent to \mathcal{T}_+ which is the transpose operator used in introducing the time-reversal symmetry, also known as TRS^\dagger [36, 87, 88]. Equivalently, instead of \mathcal{W}_g , I can introduce an operator (M_g) which changes the sign of nonHermiticity parameters such that $M_g^{-1} g M_g = -g$. The non-Hermitian composite symmetry can be readily reduced to the Hermitian Hidden symmetry $\Upsilon_H = \sigma_x \mathcal{K} \mathcal{T}_{\hat{x}}$ [26] after imposing $\mathcal{W}_g = 1$ in the Hermitian limit.

Considering the right wave-function of the system at the X points as $|\psi_X^R\rangle$ and acting the $\Upsilon_R \cdot \Upsilon_L$ on this wave-function gives $\Upsilon_R \cdot \Upsilon_L |\psi_X^R\rangle = \mathcal{T}_{2\hat{x}} |\psi_X^R\rangle = e^{-2i x_X} |\psi_X^R\rangle = -|\psi_X^R\rangle$, where I set the x component of the X points as $x_X = \pm\pi/2$. This emphasizes that $\Upsilon_R \cdot \Upsilon_L$ at nondefective degeneracies is nonunity.

nondefective degeneracies at nonzero (t_1, g_a, g_b, v) .— Switching on \mathcal{H}_1 or \mathcal{H}_2 violates the Υ symmetry and lifts the degeneracy at (at least two) X points; see the SM for details [83]. Here nonvanishing $\mathcal{H}_{1,2}$ gives rise to an effective mass term opening a gap at one or both pairs of $X_{1,2}$ nodal points; see the inset of Fig. 1. When $v_1 = -2t_1(\cosh(g_a) + \cosh(g_b))$ the gap closes at X_1 and hence, the system respects Υ at this point. Similarly, the nondefective degeneracy at X_2 is retrieved when $v_2 = 2t_1(\cosh(g_a) + \cosh(g_b))$. I present an example of this situation in Fig. 2(c,d). Notably, the observed gapless phases at v_1 and v_2 delineate the phase boundaries between two insulating phases, namely, a band insulator and a topological insulator [83].

nondefective degeneracies at $v = g_x = g_y = 0$ and $\gamma \in \{0, \pi/2\}$.— I now study systems at $v = g_x = g_y = 0$ such that the total Hamiltonian consists of $\mathcal{H} = \mathcal{H}_0 + \mathcal{H}_1$. Considering $0 < \gamma < \pi/2$ the spectrum of this system is gapped. To be precise, it possesses finite gaps in its real component and has gapless behavior in its imaginary part. However, when $\gamma \in \{0, \pi/2\}$, the system hosts only defective EPs with nonzero (g_x, g_y) while it exhibits both defective and nondefective degeneracies when $g_x = g_y = 0$; see the SM for more details [83].

Fig. 2(e,f) presents the spectrum at $\gamma = 0$ displaying both defective (magenta points) and nondefective (black points) degeneracies around the M points when $g_x = g_y = 0$, $g_a = 0.5$ and $g_b = 0.3$. I witness defective degeneracies that result in the bifurcation of the real and imaginary parts of the spectra. I also mark nondefective degeneracies with black points in these figures. The symmetry which protects the nondefective

degeneracies reads $\Upsilon'_R = \sigma_x \mathcal{K} \mathcal{W}_{g_a=g_b} \mathcal{R}_x \mathcal{T}_{\hat{x}}$, where \mathcal{R}_x performs the mirror reflection operation along the x axis such that $\mathcal{R}_x(k_x, k_y) \mathcal{R}_x^{-1} = (k_x, -k_y)$. Here, the Wick's rotation acts as $\mathcal{W}_{\mathcal{R}_{g_a=g_b}}^{-1} g_a \mathcal{W}_{\mathcal{R}_{g_a=g_b}} = i g_b$ and $\mathcal{W}_{\mathcal{R}_{g_a=g_b}}^{-1} g_b \mathcal{W}_{\mathcal{R}_{g_a=g_b}} = i g_a$. Defining the right eigenvector at the M points as $|\psi_M^R\rangle$, I find $\Upsilon'_R \cdot \Upsilon'_L |\psi_M^R\rangle = -\mathcal{T}_{2\hat{x}} |\psi_M^R\rangle = -|\psi_M^R\rangle$, where I have used $\sigma_x \mathcal{R}_x = -\mathcal{R}_x \sigma_x$. In the Hermitian limit, Υ' acts similar to the Hidden symmetry introduced in Ref. [26]. Notably, the asymptotic behavior of the Hamiltonian close to nondefective degeneracies is quadratic in momenta resulting in the non-Hermitian generalization of quadratic double-Weyl semimetals [89–92].

Setting $\gamma = \pi/2$ and $g_a = g_b = 0$, the system again exhibits both defective (magenta points) and nondefective (black points) exceptional points, but in this case in the vicinity of the Γ points, shown in Fig. 2(g,h). The system in this parameter regime is invariant under the composite symmetry operator given by $\Upsilon''_R = (e^{2i\gamma})^{i_y} (e^{-2i\gamma})^{i_x} \sigma_x \mathcal{K} \mathcal{W}_{g_a=g_b} \mathcal{R}_x \mathcal{T}_{\hat{x}}$, where (i_x, i_y) denote the real-space coordinate of site i . I note that $\mathcal{T}_{\hat{x}} i_x \mathcal{T}_{\hat{x}} = (i_x + \hat{x}) \mathcal{T}_{2\hat{x}}$ and the mirror reflection symmetry with respect to the x axis results in $\mathcal{R}_x i_y \mathcal{R}_x = -i_y$. I thereby obtain $\Upsilon''_R \cdot \Upsilon''_L = -1$ at the Γ point. Similar to systems at $\gamma = 0$, the Hamiltonian close to the nondefective degeneracies is asymptotically quadratic in momenta.

Conclusion.— I have proved a theorem stating that anti-unitary symmetries protect all nondefective twofold degeneracies in non-Hermitian systems. I have further exemplified the derivations by exploring the protection of nondefective degeneracies in a 2D tight-binding model with nonreciprocal hopping amplitudes. I have demonstrated that the anti-unitary symmetries constitute various discrete and spatial operations combined with Wick's rotations in the nonreciprocal parameter space. These findings establish the new path to the symmetry-protection of non-Hermitian degeneracies beyond the convention of discrete [44, 75, 76, 78, 93, 94] or point-group [80] symmetries for defective EPs. Further works should elaborate on the role of the composite symmetries in stabilizing nondefective degeneracies in many-body non-Hermitian systems beyond the commonly studied discrete symmetries [42, 79, 95–97]. It is also intriguing to explore the robustness of symmetry-protected nondefective degeneracies under small symmetry-breaking perturbations in interacting non-Hermitian systems.

Acknowledgment.— I acknowledge the helpful discussion with Jose L. Lado. I also thank the Galileo Galilei Institute for Theoretical Physics for hospitality during the completion of this work.

Appendix A: Conservation of symmetry operators

In the following, I present the relations whose satisfaction ensures the conservation of an operator in time. I derive these relations for Hermitian and non-Hermitian systems.

1. Hermitian systems

A Hermitian system is described by $H_H|\psi_n\rangle = \epsilon_n|\psi_n\rangle$, where H_H is a generic Hermitian Hamiltonian with eigenvalue ϵ_n and eigenvector $|\psi_n\rangle$. For this Hamiltonian, the operator \mathcal{O} is a symmetry operator if it is conserved in time. This quest is translated into

$$\partial_t\langle\mathcal{O}(t)\rangle = \langle\psi_n(t)|\mathcal{H}_H^\dagger\mathcal{O} - \mathcal{O}\mathcal{H}_H|\psi_n(t)\rangle = 0, \quad (\text{A1})$$

where I used $|\psi_n(t)\rangle = \exp(-i\mathcal{H}_H t)|\psi_n(0)\rangle$. The Hermiticity of \mathcal{H}_H then simplifies the above relation as

$$\mathcal{H}_H^\dagger\mathcal{O} - \mathcal{O}\mathcal{H}_H = 0, \quad (\text{A2})$$

$$[\mathcal{H}_H, \mathcal{O}] = 0. \quad (\text{A3})$$

Hence, \mathcal{O} is a conserved quantity in Hermitian systems if $[\mathcal{H}_H, \mathcal{O}] = 0$.

2. Non-Hermitian systems

A non-Hermitian system is described by

$$\mathcal{H}_{\text{nH}}|\psi_n^R\rangle = \epsilon_n|\psi_n^R\rangle, \quad \mathcal{H}_{\text{nH}}^\dagger|\psi_n^L\rangle = \epsilon_n^*|\psi_n^L\rangle, \quad (\text{A4})$$

where \mathcal{H}_{nH} is a non-Hermitian Hamiltonian and $\{(\epsilon_n, |\psi_n^R\rangle, |\psi_n^L\rangle)\}$ describes the non-Hermitian eigensystem with $\langle\psi_n^L|\psi_n^R\rangle = \delta_{mn}$ and $\sum_n |\psi_n^R\rangle\langle\psi_n^L| = 1$.

Based on the biorthogonality of the eigenvectors, I define the biorthogonal operator $\mathcal{O} \equiv (\mathcal{O}^R, \mathcal{O}^L)$. This operator is conserved in time when its elements satisfy

$$\begin{cases} \partial_t\langle\mathcal{O}^R(t)\rangle^{RR} &= \langle\psi^R(t)|\mathcal{H}_{\text{eff}}^\dagger\mathcal{O}^R - \mathcal{O}^R\mathcal{H}_{\text{eff}}|\psi^R(t)\rangle = 0, \\ \partial_t\langle\mathcal{O}^L(t)\rangle^{LL} &= \langle\psi^L(t)|\mathcal{H}_{\text{eff}}\mathcal{O}^L - \mathcal{O}^L\mathcal{H}_{\text{eff}}^\dagger|\psi^L(t)\rangle = 0, \end{cases} \quad (\text{A5})$$

where $\langle A \rangle^{RR(LL)}$ is the shortened notation for the expectation value $\langle\psi^{R(L)}|A|\psi^{R(L)}\rangle$. Here I used $|\psi^R(t)\rangle = \exp(-i\mathcal{H}_{\text{nH}}t)|\psi^R(0)\rangle$ and $|\psi^L(t)\rangle = \exp(-i\mathcal{H}_{\text{nH}}^\dagger t)|\psi^L(0)\rangle$.

Thereby, to keep this set of symmetry operators stationary in time, the pair of operators should fulfill

$$\begin{cases} \mathcal{H}_{\text{nH}}^\dagger\mathcal{O}^R - \mathcal{O}^R\mathcal{H}_{\text{nH}} = 0, \\ \mathcal{H}_{\text{nH}}\mathcal{O}^L - \mathcal{O}^L\mathcal{H}_{\text{nH}}^\dagger = 0. \end{cases} \quad (\text{A6})$$

I have employed this set of relations in the main text to prove the theorem.

Appendix B: Various phases and degeneracies in our tight-binding model

In the main text, I present the nondefective degeneracies which may emerge in our tight-binding model. Here I provide further details on other degeneracies and various phases in our model.

1. Non-Hermitian linear Weyl semimetal at

$$t_1 = g_a = g_b = v = 0$$

Setting $t_1 = g_a = g_b = v = 0$ in Eq. (16), the Hamiltonian casts

$$\mathcal{H}(\mathbf{k}) = \begin{pmatrix} a_{\mathbf{k}}^\dagger & b_{\mathbf{k}}^\dagger \end{pmatrix} h_{\mathbf{k}} \begin{pmatrix} a_{\mathbf{k}} \\ b_{\mathbf{k}} \end{pmatrix}, \quad (\text{B1})$$

$$\begin{aligned} &= [-2te^{-g_x - i\gamma} \cos(k_x) - 2te^{-g_y + i\gamma} \cos(k_y)] a_{\mathbf{k}}^\dagger b_{\mathbf{k}} \\ &+ [-2te^{g_x + i\gamma} \cos(k_x) - 2te^{g_y - i\gamma} \cos(k_y)] b_{\mathbf{k}}^\dagger a_{\mathbf{k}}. \end{aligned} \quad (\text{B2})$$

The dispersion relation of the system then reads

$$\epsilon_{\pm} = \pm \sqrt{fe^{\phi} + fe^{-\phi} + 2(\cos(2k_x) + \cos(2k_y) + 2)}, \quad (\text{B3})$$

with $\phi = 2i\gamma + g_x - g_y$ and $f = 4\cos(k_x)\cos(k_y)$. To identify degenerate points in the spectrum, one can use the discriminant of the two-band systems given by $\eta = fe^{\phi} + fe^{-\phi} + 2(\cos(2k_x) + \cos(2k_y) + 2)$. I present the streamlines of $(\text{Re}[\eta], \text{Im}[\eta])$ in Fig. S1(a,d,g).

Fig. S1 presents the real and imaginary parts of the spectrum for $\gamma \in \{0, 0.75, \pi/2\}$, $g_x = 0.5$ and $g_y = 0.3$. Based on these results, I can identify three possibilities.

i) The first situation happens when $|\epsilon_{\pm}|^2$ is fully real when the Peierls phase vanishes, i.e., at $\gamma = n\pi$ with $n \in \mathbb{R}$. I illustrate the streamlines of the vector field $(\text{Re}[\eta], \text{Im}[\eta])$ by teal arrows in Fig. S1(a). Evidently, the orientation of the flow lines reverses at defective EPs when they hit $\text{Re}[\eta] = 0$ curves. In this case, along the defective exceptional curves, both real and imaginary parts of the spectrum are zero; see magenta lines in panels (b,c). The intersections between these exceptional curves with $\text{Re}[\eta] = 0$ mark nondefective degeneracies located at X points and are shown by black points in (a,b,c). As a result, the X points are continuously connected to defective EPs when $\gamma = n\pi$ with $n \in \mathbb{R}$. I also witness no changes in the flow direction at nondefective degeneracies X points; see panel (a). This is not unexpected as an even number of EPs which each reverses the stream flow, intersect at the X points, and hence, no alternation of the streamlines should be observed [43].

ii) The second situation is similar to the previously discussed case i). The only difference is that, in this situation, the coexistence of defective and nondefective

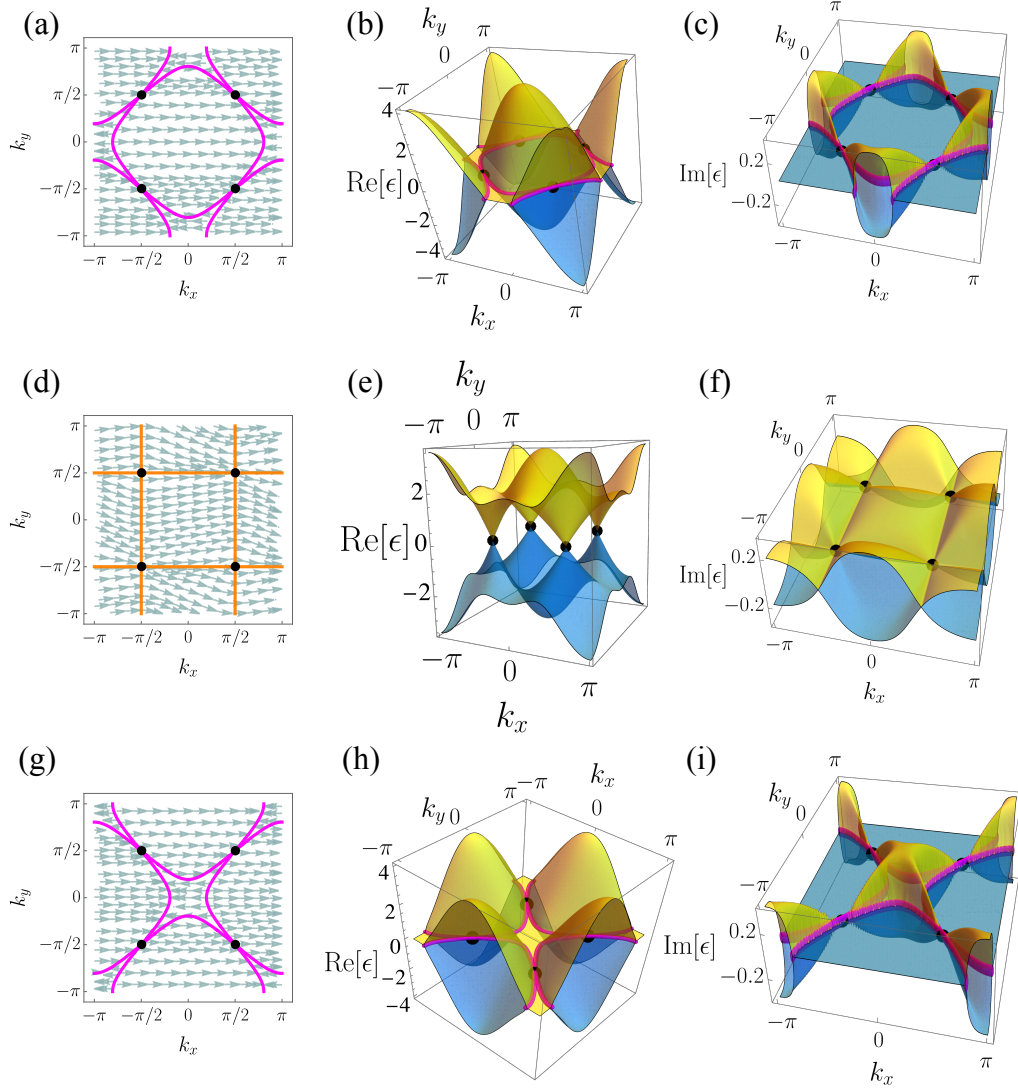


Figure S1. Stream plot of the vector field $(\text{Re}[\eta], \text{Im}[\eta])$ (a,d,g). Real (b,e,h) and imaginary (c,f,i) parts of the energy dispersion in Eq. (B3). Parameters are set to $t_1/t = g_a = g_b = v/t = 0$, $g_x = 0.5$, $g_y = 0.3$ and $\gamma = 0.00$ (a,b,c), 0.75 (d,e,f), $\pi/2$ (g,h,i). Black points depict nondefective degeneracies. Magenta (Orange) lines display $\text{Re}[\eta] = 0$ ($\text{Im}[\eta] = 0$).

degeneracies, appears when $\gamma = n\pi/2$ with odd n values, see Fig. S1(g, h, i).

iii) The third possibility occurs when $|\epsilon_{\pm}|^2$ is complex-valued with $0 < \gamma < \pi/2$. While here, the imaginary part of the spectrum exhibits i-Fermi states, along which $\text{Im}[\epsilon_{\pm}] = 0$, the real part of the dispersion relation vanishes merely at nondefective degeneracies the X points. Note that these degeneracies are isolated, and they are no longer the termination points of i-Fermi arcs due to the absence of r-Fermi arcs, along which $\text{Re}[\epsilon_{\pm}] = 0$ [43].

As it is evident from Fig. S1, the nondefective degeneracies at the X points are robust against any changes of (γ, g_x, g_y) values. This is because our model respects a composite symmetry discussed in the main text.

The asymptotic behavior of the Hamiltonian close to the nondefective degeneracies reads $h_{\mathbf{k}}^{\text{lin}} = \mathbf{d} \cdot \boldsymbol{\sigma}$ where

$d_x = -s[2t(k_y \cosh(g_y - i\gamma) - k_x \cosh(g_x + i\gamma))]$, $d_y = 2its(k_y \sinh(g_y - i\gamma) - k_x \sinh(g_x + i\gamma))$ and $d_z = 0$ with $s = +1(-1)$ at $X_1(X_2)$. The energy dispersion relation then yields

$$\epsilon_X^{\text{lin}} = \mp 2t \sqrt{2sk_x k_y \cosh(2i\gamma + g_x - g_y) + k_x^2 + k_y^2}, \quad (\text{B4})$$

and the associated eigenvectors read

$$|\psi_X^{\text{lin}}\rangle = \begin{pmatrix} \pm \sqrt{\frac{e^{2i\gamma}(2sk_x k_y \cosh(2i\gamma + g_x - g_y) + k_x^2 + k_y^2)}{e^{g_y} k_y + k_x e^{g_x + 2i\gamma}}} \\ 1 \end{pmatrix}. \quad (\text{B5})$$

Moreover, $h_{\mathbf{k}}^{\text{lin}}$ can be rewritten as a linear Weyl Hamiltonian $h_{\mathbf{k}}^{\text{lin}} = M_{ij} p^i \sigma^j$ where M is a matrix with complex-

valued elements. This Hamiltonian resembles the Hermitian linear Weyl model [26]. For this reason, I dub the system in this parameter regime "the non-Hermitian linear Weyl semimetals."

2. Non-Hermitian trivial and topological insulators by keeping either (t_1, g_a, g_b) or v nonzero

After turning on \mathcal{H}_1 or \mathcal{H}_2 , the Hamiltonian $h_{\mathbf{k}}$ in Eq. (B2) casts $h_{\mathbf{k}} = \mathbf{d} \cdot \boldsymbol{\sigma}$ where $d_0 = -4it_1 \sin(k_y) \sinh(g_a/2 - g_b/2) \cosh(g_a/2 + g_b/2 + ik_x)$, $d_x = -2t \cos(k_x) \cosh(g_x + i\gamma) - 2t \cos(k_y) \cosh(g_y - i\gamma)$, $d_y = 2it \cos(k_x) \sinh(g_x + i\gamma) + 2it \cos(k_y) \sinh(g_y - i\gamma)$ and

$$d_z = 2t_1 (\cosh(g_a) + \cosh(g_b)) \sin(k_x) \sin(k_y) - 2it_1 (\sinh(g_a) + \sinh(g_b)) \cos(k_x) \sin(k_y) + v. \quad (\text{B6})$$

Here nonvanishing d_z gives rise to an effective mass term, which lifts the degeneracy at, at least two of the X points. The gap closure occurs when

$$v_1 = -2t_1 (\cosh(g_a) + \cosh(g_b)), \quad (\text{B7})$$

$$v_2 = 2t_1 (\cosh(g_a) + \cosh(g_b)). \quad (\text{B8})$$

When $v = v_1$, the gap closes at X_1 . Hence, the system respects the composite symmetry Υ at this point; see the main text. Similarly, the nondefective degeneracy at X_2 is retrieved when $v = v_2$; see also Fig. 2(c,d) in the main text.

Fig. S2(a) displays the phase diagram of our system where the phase boundaries $v_{1,2}$ (teal surfaces) separate the non-Hermitian band insulator (yellow region) from the non-Hermitian topological insulator. I set $g_a = g_b$ in Fig. S2(a). The complex-valued band structure for the topological insulator with a nonzero gap is exemplified in Fig. S2(b,c).

By imposing open boundary conditions along x or y axis, I can identify chiral edge modes shown in red in Fig. S3(a,b) and (e,f), respectively. These chiral edge modes have finite lifetime (imaginary parts) for momenta deep inside the gap when the system is merely periodic along the y axis. However, when periodicity is respected only along the x axis, the chiral edge modes possess zero imaginary parts inside the gap region away from the bulk states (blue curves). The chiral edge modes in both cases are localized at opposite boundaries of the system, as can be seen from the absolute values of eigenvectors, shown in (c,g), at $i = 30, 31$ associated with $\epsilon_i = 0.0$. I further observe the skin effect, the localization of bulk modes at boundaries, e.g., in panel (c, h), due to the reciprocity (nonzero (g_a, g_b)). The observed skin effect in panel (h) is also known as the Z_2 skin effect [36] protected by the time-reversal symmetry. I note that the absence of the skin effect at $k_y = 0$ in panel (d) and at $k_x = \pi/2$ in panel (g) is due to the zero imaginary parts

of all modes resulting in delocalizing the bulk states, similar to Hermitian systems.

3. Non-Hermitian quadratic double Weyl semimetals at $v = 0$ and $\gamma \in \{0, \pi/2\}$

Imposing $v = 0$ turns off \mathcal{H}_2 and subsequently, the Hamiltonian casts $h_{\mathbf{k}} = d_0 \mathbb{1} + d_x \sigma_x + d_z \sigma_z$ where

$$d_0 = -4it_1 \sin(k_y) \sinh\left(\frac{g_a - g_b}{2}\right) \cosh\left(\frac{g_a + g_b + 2ik_x}{2}\right), \quad (\text{B9})$$

$$d_x = 2it [\cos(k_x) \sinh(g_x + i\gamma) + \cos(k_y) \sinh(g_y - i\gamma)], \quad (\text{B10})$$

$$d_z = 2t_1 \sin(k_y) [\sin(k_x) (\cosh(g_a) + \cosh(g_b)) - i \cos(k_x) (\sinh(g_a) + \sinh(g_b))]. \quad (\text{B11})$$

The associated dispersion relations then reads $\epsilon_{\pm} = d_0 \pm \sqrt{\eta}$ with $\eta = d_x^2 + d_z^2$. I present the stream plot of $(\text{Re}[\eta], \text{Im}[\eta])$ in Fig. S4 at $t_1/t = 0.75$, $g_a = 0.5$, $g_b = 0.3$, $g_x = g_y = 0$, and $\gamma = 0$ (a) and $\pi/2$ (b). I also plot Fig. S4(c,d) with $t_1/t = 0.75$, $g_a = 0.5$, $g_b = 0.3$, $g_x = 0.2$, $g_y = 0.1$ and $\gamma = 0$ (c) and $\pi/2$ (d). Fig. S4 further displays $\text{Re}[\eta] = 0$ in magenta and $\text{Im}[\eta] = 0$ in orange lines. The intersection of these lines identifies defective EPs in our systems. When even numbers of these lines cross, I detect nondefective degeneracies marked in black points in (a,b). These nondefective degeneracies locate at the M points when $\gamma = 0$, and they appear at the Γ points at $\gamma = \pi/2$; see also the discussion in the main text. I emphasize that these nondefective degeneracies disappear when nonreciprocal nearest neighbor hopping parameters, namely (g_x, g_y) , are nonzero, as shown in (c,d). The energy band associated with parameters in Fig. S4(c,d) are shown in Fig. S5. Unsurprisingly, transitioning from one gapless phase to the other is through a gapped phase with $0 < \gamma < \pi/2$.

Around nondefective degeneracies, the Hamiltonian is asymptotically quadratic in momentum as it casts $h_{\mathbf{k}}^{\text{quad}} = \mathbf{d}^{\text{quad}} \cdot \boldsymbol{\sigma}$ where

$$d_0^{\text{quad}} = 2p_y t_1 [-i(\sinh(g_a) - \sinh(g_b)) + p_x \cosh(g_a) - p_x \cosh(g_b)], \quad (\text{B12})$$

$$d_x^{\text{quad}} = t [(p_x^2 - 2) \cosh(g_x) + (p_y^2 - 2) \cosh(g_y)], \quad (\text{B13})$$

$$d_y^{\text{quad}} = -it [(p_x^2 - 2) \sinh(g_x) + (p_y^2 - 2) \sinh(g_y)], \quad (\text{B14})$$

$$d_z^{\text{quad}} = 2p_y t_1 [p_x (\cosh(g_a) + \cosh(g_b)) - i(\sinh(g_a) + \sinh(g_b))], \quad (\text{B15})$$

where $\mathbf{p} = \mathbf{k} - M$, $\gamma = 0$ and nondefective degeneracies are located at the M points. When $\gamma = \pi/2$ and nondefective degeneracies reside at the Γ points, different

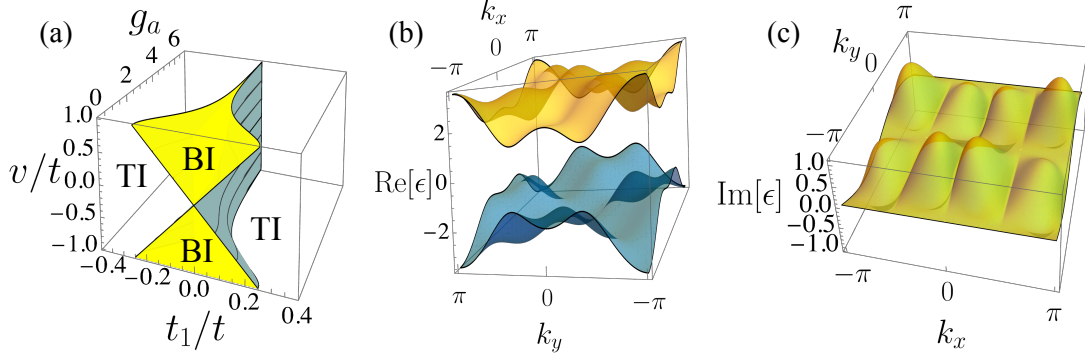


Figure S2. (a) The phase diagram of the system comprises the band insulating (BI), yellow regions, and topological insulating (TI) phases at $g_a = g_b$ and with nonzero t_1 and v . The teal surfaces in (a) separating BI and TI phases depict v_1 and v_2 given in Eqs. (B7, B8). Real (b) and imaginary (c) parts of the energy dispersion of $h_{\mathbf{k}}$ at $t_1/t = 0.75$, $g_a = 0.5$, $g_b = 0.3$ $v/t = g_x = g_y = 0.0$ and $\gamma = 0.5$.

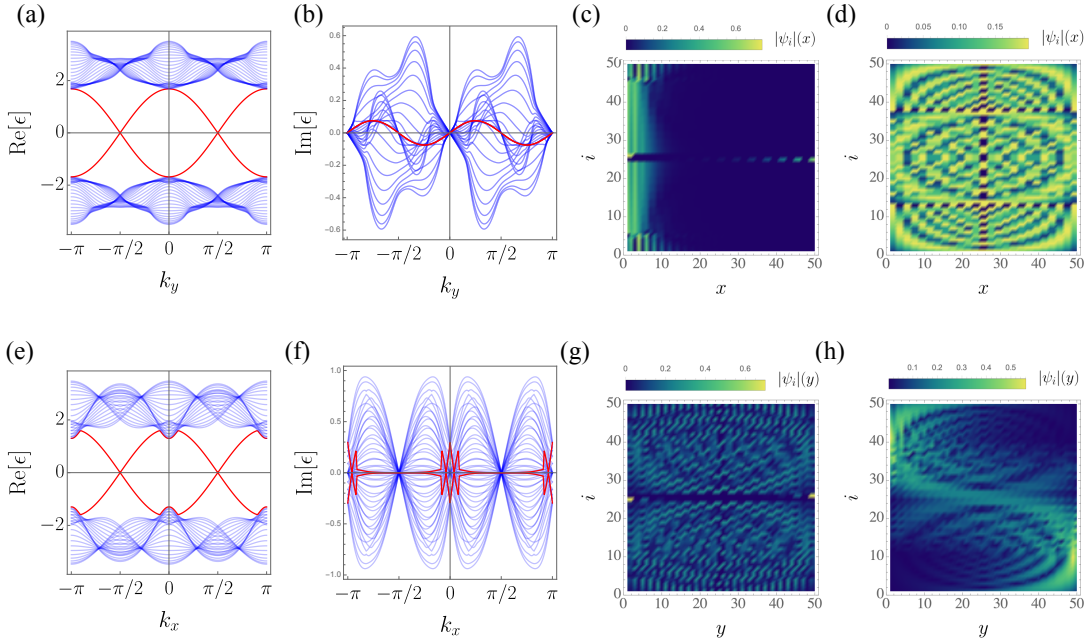


Figure S3. Real (a) and imaginary (b) parts of the spectrum with open (periodic) boundary conditions along the x (k_y)-axis. The absolute values of eigenvectors $|\psi_i|$ associated with eigenvalue ϵ_i , sorted ascendingly with respect to $\text{Re}[\epsilon_i]$, for the system presented in (a,b) at $k_y = \pi/2$ (c) and 0 (d). (e,f) Similar to (a,b) but with open (periodic) boundary conditions along the y (k_x)-axis. The absolute values of eigenvectors for the system are presented in (e,f) at $k_x = \pi/2$ (g) and 0 (h). All plots are obtained at $t_1/t = 0.75$, $g_a = 0.5$, $g_b = 0.3$ $v/t = g_x = g_y = 0.0$ and $\gamma = 0.5$.

components of $h_{\mathbf{p}}^{\text{quad}}$ with $\mathbf{p} = \mathbf{k} - \Gamma$ yield

$$d_0^{\text{quad}} = 2p_y t_1 [-i(\sinh(g_a) - \sinh(g_b)) + p_x \cosh(g_a) - p_x \cosh(g_b)], \quad (\text{B16})$$

$$d_x^{\text{quad}} = it [(p_x^2 - 2) \sinh(g_x) - (p_y^2 - 2) \sinh(g_y)], \quad (\text{B17})$$

$$d_y^{\text{quad}} = t [(p_x^2 - 2) \cosh(g_x) - (p_y^2 - 2) \cosh(g_y)], \quad (\text{B18})$$

$$d_z^{\text{quad}} = 2p_y t_1 [p_x (\cosh(g_a) + \cosh(g_b)) - i(\sinh(g_a) + \sinh(g_b))]. \quad (\text{B19})$$

These systems are the non-Hermitian generalizations of the quadratic double Weyl semimetals [89–92].

After understanding our model with the periodic boundary conditions in this parameter regime, I now explore the underlying physics when periodicity along the x or y axis is lifted; See real and imaginary components of the energy spectra in panels (a,b) in Figs. S6, S7, S8 and S9. Here Figs. S6 and S7 are plotted at $\gamma = 0$ and Figs. S8 and S9 are obtained at $\gamma = \pi/2$. Evidently, these two sets of results are very similar to each other. Both cases exhibit boundary modes with nearly zero real

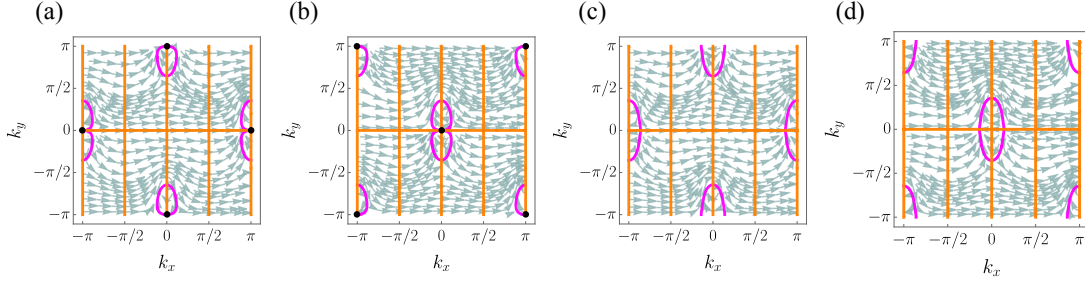


Figure S4. The stream plot of the vector field $(\text{Re}[\eta], \text{Im}[\eta])$ depicted by teal arrows, I present $\text{Re}[\eta] = 0$ in magenta solid line and $\text{Im}[\eta] = 0$ in orange. Black points indicate nondefective degeneracies. The intersecting points between magenta and orange lines locate defective EPs. All plots are obtained at $t_1/t = 0.75$, $g_a = 0.5$, $g_b = 0.3$ $v/t = 0.0$. I set $g_x = g_y = 0.0$ and $\gamma = 0.0$ in (a), $g_x = g_y = 0.0$ and $\pi/2$ in (b), $g_x = 0.2$, $g_y = 0.1$ and $\gamma = 0.0$ in (c) and $g_x = 0.2$, $g_y = 0.1$ and $\gamma = \pi/2$ in (d).

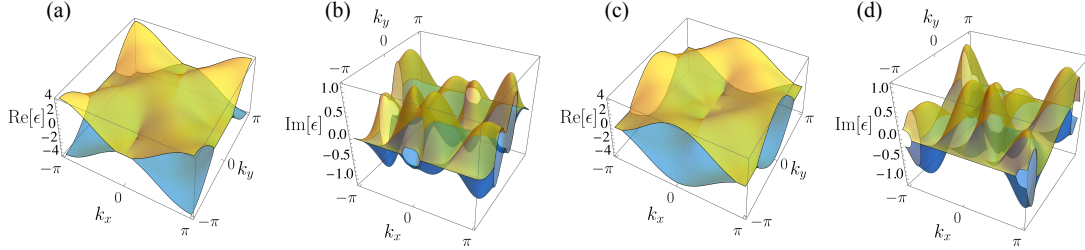


Figure S5. Real (a,c) and imaginary (b,d) components of the band structure for systems at $t_1/t = 0.75$, $g_a = 0.5$, $g_b = 0.3$ $v/t = 0.0$, $g_x = 0.2$, $g_y = 0.1$ and $\gamma = 0.0$ (a,b) and $\gamma = \pi/2$ (c,d).

and imaginary parts when periodicity along the k_y axis is relaxed. On the contrary, the boundary modes possess finite imaginary parts when one enforces the open boundary conditions along the x axis. The behavior of eigenvectors in these parameter regimes is similar to those discussed in Sec. B 2. The only major difference is how eigenvectors behave at two zero eigen-energies ($\epsilon_i = 0.0$) with $i = 30, 31$ in panels (c) in Figs. S6, S7, S8, and S9. For these two eigenvalues, in contrast to the results of Sec. B 2, I realize that the associated eigenvectors coalesce. Hence, I conclude that these systems with open boundary conditions along the y and x axes experience defective EPs at $k_x = \pi/2$ and $k_y = \pi/2$, respectively. I also observe the localization of the bulk eigenvectors, i.e., the skin effect, around $x = 0$; see Figs. S7 and S9. However, the bulk eigenvectors are localized at the left/right ends of the system along the y -axis when periodicity along k_y is relaxed.

* sharareh.sayyad@mpl.mpg.de

- [1] Stefan Imhof, Christian Berger, Florian Bayer, Johannes Brehm, Laurens W. Molenkamp, Tobias Kiessling, Frank Schindler, Ching Hua Lee, Martin Greiter, Titus Neupert, and Ronny Thomale, “Topoelectrical-circuit realization of topological corner modes,” *Nature Physics* **14**, 925–929 (2018), [arXiv:1708.03647](#).
- [2] Tejas Kotwal, Fischer Moseley, Alexander Stegmaier,

- Stefan Imhof, Hauke Brand, Tobias Kießling, Ronny Thomale, Henrik Ronellenfitsch, and Jörn Dunkel, “Active topoelectrical circuits,” *Proceedings of the National Academy of Sciences of the United States of America* **118** (2021), [arXiv:1903.10130](#).
- [3] Linhu Li, Sen Mu, Ching Hua Lee, and Jiangbin Gong, “Quantized classical response from spectral winding topology,” *Nature Communications* **12**, 1–11 (2021), [arXiv:2012.08799](#).
- [4] H. Miao, L.-M. Wang, P. Richard, S.-F. Wu, J. Ma, T. Qian, L.-Y. Xing, X.-C. Wang, C.-Q. Jin, C.-P. Chou, Z. Wang, W. Ku, and H. Ding, “Coexistence of orbital degeneracy lifting and superconductivity in iron-based superconductors,” *Phys. Rev. B* **89**, 220503 (2014).
- [5] Fernando De Juan, Adolfo G. Grushin, Takahiro Morimoto, and Joel E. Moore, “Quantized circular photogalvanic effect in Weyl semimetals,” *Nature Communications* **8**, 1–7 (2017), [arXiv:1611.05887](#).
- [6] Duc Thanh Tran, Alexandre Dauphin, Adolfo G. Grushin, Peter Zoller, and Nathan Goldman, “Probing topology by “heating”: Quantized circular dichroism in ultracold atoms,” *Science Advances* **3**, 1–9 (2017), [arXiv:1704.01990](#).
- [7] Hannes Hübener, Michael A. Sentef, Umberto De Giovannini, Alexander F. Kemper, and Angel Rubio, “Creating stable Floquet-Weyl semimetals by laser-driving of 3D Dirac materials,” *Nature Communications* **8**, 1–8 (2017), [arXiv:1604.03399](#).
- [8] N. P. Armitage, E. J. Mele, and Ashvin Vishwanath, “Weyl and dirac semimetals in three-dimensional solids,” *Rev. Mod. Phys.* **90**, 015001 (2018).
- [9] R. Flores-Calderon and A. Martin-Ruiz, “Quantized electrochemical transport in weyl semimetals,” *Phys. Rev. B*

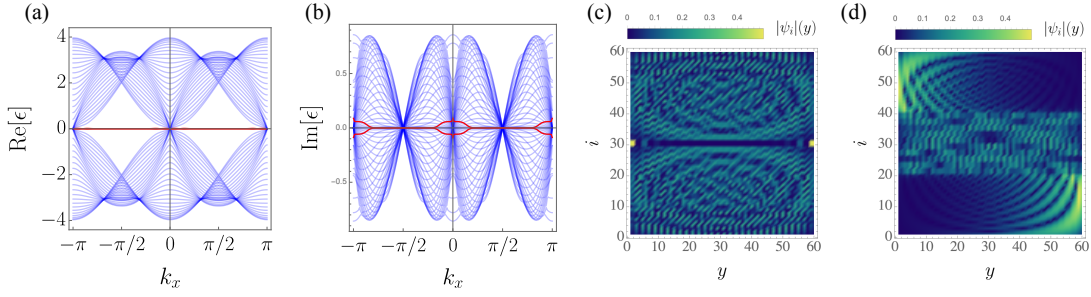


Figure S6. The real (a) and imaginary (b) parts of the spectrum with open (periodic) boundary conditions along the x (k_y)-axis. The absolute value of eigenvectors for the system presented in (a,b) at $k_x = \pi/2$ (c) and 0 (d). All plots are obtained at $t_1/t = 0.75$, $g_a = 0.5$, $g_b = 0.3$ $v/t = g_x = g_y = 0.0$ and $\gamma = 0$.

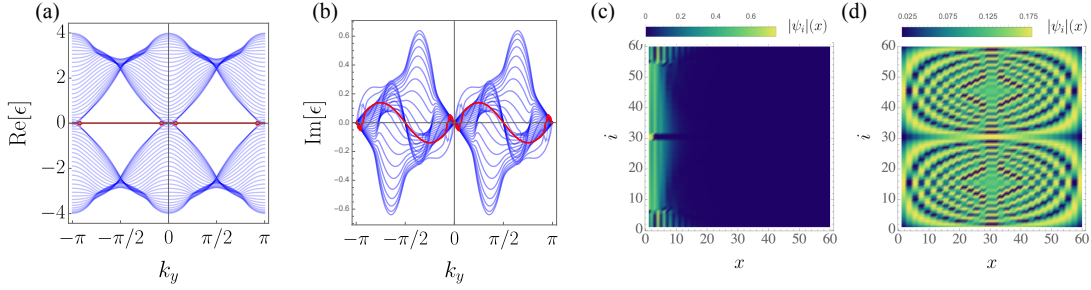


Figure S7. The same as Fig. S6 but with open (periodic) boundary conditions along the x (k_y)-axis.

- 103, 035102 (2021).**
- [10] Johannes Gooth, Anna C. Niemann, Tobias Meng, Adolfo G. Grushin, Karl Landsteiner, Bernd Gotsmann, Fabian Menges, Marcus Schmidt, Chandra Shekhar, Vicky Süß, Ruben Hühne, Bernd Rellinghaus, Claudia Felser, Binghai Yan, and Kornelius Nielsch, “Experimental signatures of the mixed axial-gravitational anomaly in the Weyl semimetal NbP,” *Nature* **547**, 324–327 (2017).
 - [11] Kamal Das and Amit Agarwal, “Thermal and gravitational chiral anomaly induced magneto-transport in weyl semimetals,” *Phys. Rev. Research* **2**, 013088 (2020).
 - [12] N. P. Ong and Sihang Liang, “Experimental signatures of the chiral anomaly in Dirac–Weyl semimetals,” *Nature Reviews Physics* **3**, 394–404 (2021).
 - [13] Chuanchang Zeng, Snehasish Nandy, and Sumanta Tewari, “Chiral anomaly induced nonlinear nernst and thermal hall effects in weyl semimetals,” *Phys. Rev. B* **105**, 125131 (2022).
 - [14] Chuanchang Zeng, Snehasish Nandy, Pu Liu, Sumanta Tewari, and Yugui Yao, “Quantum oscillations of the nonlinear planar effects signifying chiral anomaly in weyl semimetals,” (2022), 2203.01196.
 - [15] Barry Bradlyn, Jennifer Cano, Zhijun Wang, M. G. Vergniory, C. Felser, R. J. Cava, and B. Andrei Bernevig, “Beyond Dirac and Weyl fermions: Unconventional quasiparticles in conventional crystals,” *Science* **353** (2016), arXiv:1603.03093.
 - [16] Peizhe Tang, Quan Zhou, and Shou Cheng Zhang, “Multiple Types of Topological Fermions in Transition Metal Silicides,” *Physical Review Letters* **119**, 10–12 (2017), arXiv:1706.03817.
 - [17] J. Z. Ma, J. B. He, Y. F. Xu, B. Q. Lv, D. Chen, W. L. Zhu, S. Zhang, L. Y. Kong, X. Gao, L. Y. Rong, Y. B. Huang, P. Richard, C. Y. Xi, E. S. Choi, Y. Shao, Y. L. Wang, H. J. Gao, X. Dai, C. Fang, H. M. Weng, G. F. Chen, T. Qian, and H. Ding, “Three-component fermions with surface Fermi arcs in tungsten carbide,” *Nature Physics* **14**, 349–354 (2018).
 - [18] Jennifer Cano, Barry Bradlyn, and M. G. Vergniory, “Multifold nodal points in magnetic materials,” *APL Materials* **7**, 1–18 (2019), arXiv:1904.12867.
 - [19] B. Q. Lv, Z. L. Feng, J. Z. Zhao, Noah F.Q. Yuan, A. Zong, K. F. Luo, R. Yu, Y. B. Huang, V. N. Strocov, A. Chikina, A. A. Soluyanov, N. Gedik, Y. G. Shi, T. Qian, and H. Ding, “Observation of multiple types of topological fermions in PdBiSe,” *Physical Review B* **99**, 1–7 (2019), arXiv:1905.11285.
 - [20] Boyang Xie, Hui Liu, Haonan Wang, Hua Cheng, Jianguo Tian, and Shuqi Chen, “A Review of Topological Semimetal Phases in Photonic Artificial Microstructures,” *Frontiers in Physics* **9**, 1–14 (2021).
 - [21] Conyers Herring, “Accidental degeneracy in the energy bands of crystals,” *Phys. Rev.* **52**, 365–373 (1937).
 - [22] J. von Neumann and E. P. Wigner, “Über merkwürdige diskrete eigenwerte,” in *The Collected Works of Eugene Paul Wigner: Part A: The Scientific Papers*, edited by Arthur S. Wightman (Springer Berlin Heidelberg, Berlin, Heidelberg, 1993) pp. 291–293.
 - [23] Yu N. Demkov and P. B. Kurasov, “Von Neumann–Wigner theorem: Level repulsion and degenerate eigenvalues,” *Theoretical and Mathematical Physics* **153**, 1407–1422 (2007).
 - [24] Lin Xu, Hai-Xiao Wang, Ya-Dong Xu, Huan-Yang Chen, and Jian-Hua Jiang, “Accidental degeneracy in photonic bands and topological phase transitions in two-dimensional core-shell dielectric photonic crystals,” *Opt.*

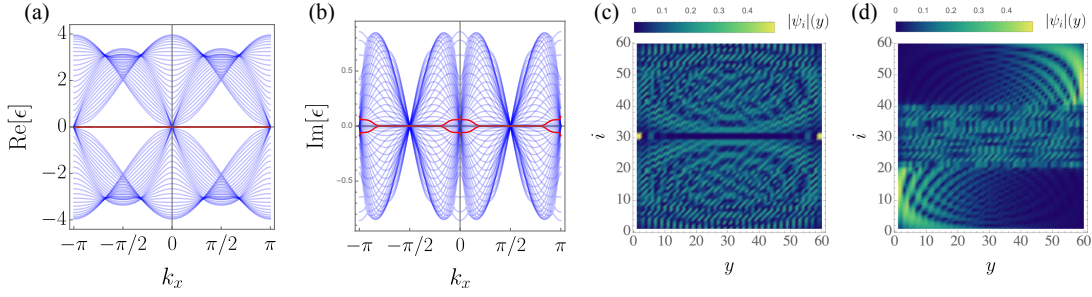


Figure S8. The same as Fig. S6 but the absolute value of eigenvectors for the system presented in (a,b) at $k_y = \pi/2$ (c) and 0 (d). For all panels I set $t_1/t = 0.75$, $g_a = 0.5$, $g_b = 0.3$ $v/t = g_x = g_y = 0.0$ and $\gamma = \pi/2$.

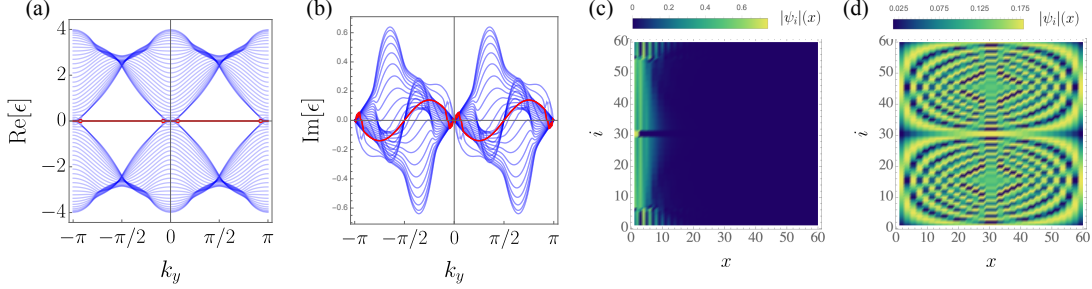


Figure S9. The same as Fig. S7 but at $t_1/t = 0.75$, $g_a = 0.5$, $g_b = 0.3$ $v/t = g_x = g_y = 0.0$ and $\gamma = \pi/2$.

Express **24**, 18059–18071 (2016).

- [25] Philip B. Allen and Warren E. Pickett, “Accidental degeneracy in k-space, geometrical phase, and the perturbation of π by spin-orbit interactions,” *Physica C: Superconductivity and its Applications* **549**, 102–106 (2018).
- [26] Jing Min Hou, “Hidden-Symmetry-Protected Topological Semimetals on a Square Lattice,” *Physical Review Letters* **111**, 1–5 (2013), [arXiv:1212.4202](#).
- [27] Jing Min Hou and Wei Chen, “Hidden symmetry-protected Z_2 topological insulator in a cubic lattice,” *Physical Review B* **96**, 1–8 (2017).
- [28] Jing Min Hou and Wei Chen, “Hidden antiunitary symmetry behind “accidental” degeneracy and its protection of degeneracy,” *Frontiers of Physics* **13**, 1–4 (2018), [arXiv:1707.05313](#).
- [29] Jing-Min Hou, “Peierls-phase-induced topological semimetals in an optical lattice: Moving of dirac points, anisotropy of dirac cones, and hidden symmetry protection,” *Chinese Physics B* **29**, 120305 (2020).
- [30] Yuto Ashida, Zongping Gong, and Masahito Ueda, “Non-hermitian physics,” *Advances in Physics* **69**, 249–435 (2020).
- [31] Emil J. Bergholtz, Jan Carl Budich, and Flore K. Kunst, “Exceptional topology of non-hermitian systems,” *Rev. Mod. Phys.* **93**, 015005 (2021).
- [32] Nobuyuki Okuma and Masatoshi Sato, “Non-hermitian topological phenomena: A review,” (2022), [2205.10379](#).
- [33] S. Lin, L. Jin, and Z. Song, “Symmetry protected topological phases characterized by isolated exceptional points,” *Phys. Rev. B* **99**, 165148 (2019).
- [34] Yongxu Fu and Shaolong Wan, “Degeneracy and defectiveness in non-hermitian systems with open boundary,” *Phys. Rev. B* **105**, 075420 (2022).
- [35] Dan S. Borgnia, Alex Jura Kruchkov, and Robert-Jan Slager, “Non-hermitian boundary modes and topology,” *Phys. Rev. Lett.* **124**, 056802 (2020).
- [36] Nobuyuki Okuma, Kohei Kawabata, Ken Shiozaki, and Masatoshi Sato, “Topological origin of non-hermitian skin effects,” *Phys. Rev. Lett.* **124**, 086801 (2020).
- [37] Kohei Kawabata, Nobuyuki Okuma, and Masatoshi Sato, “Non-Bloch band theory of non-Hermitian Hamiltonians in the symplectic class,” *Physical Review B* **101**, 195147 (2020), [arXiv:2003.07597](#).
- [38] Nobuyuki Okuma and Masatoshi Sato, “Quantum anomaly, non-hermitian skin effects, and entanglement entropy in open systems,” *Phys. Rev. B* **103**, 085428 (2021).
- [39] Xiujuan Zhang, Tian Zhang, Ming-Hui Lu, and Yan-Feng Chen, “A review on non-Hermitian skin effect,” (2022), [2205.08037](#).
- [40] Stefano Longhi, “Self-healing of non-hermitian topological skin modes,” *Phys. Rev. Lett.* **128**, 157601 (2022).
- [41] Huitao Shen, Bo Zhen, and Liang Fu, “Topological band theory for non-hermitian hamiltonians,” *Phys. Rev. Lett.* **120**, 146402 (2018).
- [42] Haoran Xue, Qiang Wang, Baile Zhang, and Y. D. Chong, “Non-hermitian dirac cones,” *Phys. Rev. Lett.* **124**, 236403 (2020).
- [43] Zhesen Yang, A. P. Schnyder, Jiangping Hu, and Ching-Kai Chiu, “Fermion doubling theorems in two-dimensional non-hermitian systems for fermi points and exceptional points,” *Phys. Rev. Lett.* **126**, 086401 (2021).
- [44] Sharareh Sayyad, Marcus Stalhammar, Lukas Rodland, and Flore K. Kunst, “Symmetry-protected exceptional and nodal points in non-hermitian systems,” (2022), [arXiv:2204.13945](#).
- [45] Jan Wiersig, “The distance between exceptional points and diabolic points and its implication for the re-

- sponse strength of non-hermitian systems,” (2022), [arXiv:2205.15685](#).
- [46] This type of degeneracies are sometimes dubbed ‘diabolic points’ or ‘nodal points’ [41, 44].
- [47] These nondefective degeneracies are also known as the ‘nondefective EPs’ [44].
- [48] Kazuki Sone, Yuto Ashida, and Takahiro Sagawa, “Exceptional non-hermitian topological edge mode and its application to active matter,” *Nature Communications* **11** (2020).
- [49] Lucas S. Palacios, Serguei Tchoumakov, Maria Guix, Ignacio Pagonabarraga, Samuel Sánchez, and Adolfo G. Grushin, “Guided accumulation of active particles by topological design of a second-order skin effect,” *Nature Communications* **12** (2021).
- [50] Motohiko Ezawa, “Electric circuits for non-hermitian chern insulators,” *Phys. Rev. B* **100**, 081401 (2019).
- [51] Tobias Hofmann, Tobias Helbig, Frank Schindler, Nora Salgo, Marta Brzezińska, Martin Greiter, Tobias Kiessling, David Wolf, Achim Vollhardt, Anton Kabaši, Ching Hua Lee, Ante Bilušić, Ronny Thomale, and Titus Neupert, “Reciprocal skin effect and its realization in a topoelectrical circuit,” *Phys. Rev. Research* **2**, 023265 (2020).
- [52] S M Rafi-Ul-Islam, Zhuo Bin Siu, and Mansoor B A Jalil, “Non-hermitian topological phases and exceptional lines in topoelectrical circuits,” *New Journal of Physics* **23**, 033014 (2021).
- [53] Jien Wu, Xueqin Huang, Yating Yang, Weiyin Deng, Jiuyang Lu, Wenji Deng, and Zhengyou Liu, “Non-hermitian second-order topology induced by resistances in electric circuits,” *Phys. Rev. B* **105**, 195127 (2022).
- [54] Christoph Fleckenstein, Alberto Zorzato, Daniel Varjas, Emil J. Bergholtz, Jens H. Bardarson, and Apoorv Tiwari, “Non-hermitian topology in monitored quantum circuits,” *Phys. Rev. Research* **4**, L032026 (2022).
- [55] Constantinos Valagiannopoulos and Vassilios Kovanis, “Engineering the emission of laser arrays to nullify the jamming from passive obstacles,” *Photon. Res.* **6**, A43–A50 (2018).
- [56] Changqing Wang, Zhoutian Fu, and Lan Yang, “Non-hermitian physics and engineering in silicon photonics,” in *Silicon Photonics IV: Innovative Frontiers*, edited by David J. Lockwood and Lorenzo Pavesi (Springer International Publishing, Cham, 2021) pp. 323–364.
- [57] Midya Parto, Yuzhou G. N. Liu, Babak Bahari, Mercedeh Khajavikhan, and Demetrios N. Christodoulides, “Non-hermitian and topological photonics: optics at an exceptional point,” *Nanophotonics* **10**, 403–423 (2021).
- [58] Yabin Jin, Wenxin Zhong, Runcheng Cai, Xiaoying Zhuang, Yan Pennec, and Bahram Djafari-Rouhani, “Non-hermitian skin effect in a phononic beam based on piezoelectric feedback control,” *Applied Physics Letters* **121**, 022202 (2022).
- [59] Constantinos Valagiannopoulos, “Stable electromagnetic interactions with effective media of active multilayers,” *Phys. Rev. B* **105**, 045304 (2022).
- [60] Jing-jing Liu, Zheng-wei Li, Ze-Guo Chen, Weiyan Tang, An Chen, Bin Liang, Guancong Ma, and Jian-Chun Cheng, “Experimental realization of weyl exceptional rings in a synthetic three-dimensional non-hermitian phononic crystal,” *Phys. Rev. Lett.* **129**, 084301 (2022).
- [61] Javier del Pino, Jesse J. Slim, and Ewold Verhagen, “Non-hermitian chiral phononics through optomechanically induced squeezing,” *Nature* **606**, 82–87 (2022).
- [62] B. Peng, Ş. K. Özdemir, S. Rotter, H. Yilmaz, M. Liertzer, F. Monifi, C. M. Bender, F. Nori, and L. Yang, “Loss-induced suppression and revival of lasing,” *Science* **346**, 328–332 (2014).
- [63] Liang Feng, Zi Jing Wong, Ren-Min Ma, Yuan Wang, and Xiang Zhang, “Single-mode laser by parity-time symmetry breaking,” *Science* **346**, 972–975 (2014).
- [64] H. Hodaei, M. A. Miri, A. U. Hassan, W. E. Hayenga, M. Heinrich, D. N. Christodoulides, and M. Khajavikhan, “Parity-time-symmetric coupled microring lasers operating around an exceptional point,” *Opt. Lett.* **40**, 4955–4958 (2015).
- [65] Jean Alexandre, Peter Millington, and Dries Seneaeve, “Consistent description of field theories with non-hermitian mass terms,” *Journal of Physics: Conference Series* **952**, 012012 (2018).
- [66] Sharareh Sayyad, Julia D. Hannukainen, and Adolfo G. Grushin, “Non-hermitian chiral anomalies,” *Phys. Rev. Research* **4**, L042004 (2022).
- [67] Kohei Kawabata, Ken Shiozaki, and Shinsei Ryu, “Topological field theory of non-hermitian systems,” *Phys. Rev. Lett.* **126**, 216405 (2021).
- [68] Stefano Longhi, “Non-hermitian bidirectional robust transport,” *Phys. Rev. B* **95**, 014201 (2017).
- [69] Lei Du, Yan Zhang, and Jin-Hui Wu, “Controllable unidirectional transport and light trapping using a one-dimensional lattice with non-hermitian coupling,” *Scientific Reports* **10** (2020).
- [70] Hamed Ghaemi-Dizicheh and Henning Schomerus, “Compatibility of transport effects in non-hermitian non-reciprocal systems,” *Phys. Rev. A* **104**, 023515 (2021).
- [71] Selma Franca, Viktor Könye, Fabian Hassler, Jeroen van den Brink, and Cosma Fulga, “Non-hermitian physics without gain or loss: The skin effect of reflected waves,” *Phys. Rev. Lett.* **129**, 086601 (2022).
- [72] Sharareh Sayyad, Jinlong Yu, Adolfo G. Grushin, and Lukas M. Sieberer, “Entanglement spectrum crossings reveal non-hermitian dynamical topology,” *Phys. Rev. Research* **3**, 033022 (2021).
- [73] Liang-Jun Zhai, Guang-Yao Huang, and Shuai Yin, “Nonequilibrium dynamics of the localization-delocalization transition in the non-hermitian aubry-andré model,” *Phys. Rev. B* **106**, 014204 (2022).
- [74] Elias Starchl and Lukas M. Sieberer, “Relaxation to a parity-time symmetric generalized gibbs ensemble after a quantum quench in a driven-dissipative kitaev chain,” (2022), [arXiv:2203.14589](#).
- [75] Tsuneya Yoshida, Robert Peters, Norio Kawakami, and Yasuhiro Hatsugai, “Symmetry-protected exceptional rings in two-dimensional correlated systems with chiral symmetry,” *Phys. Rev. B* **99**, 121101 (2019).
- [76] Pierre Delpace, Tsuneya Yoshida, and Yasuhiro Hatsugai, “Symmetry-protected multifold exceptional points and their topological characterization,” *Phys. Rev. Lett.* **127**, 186602 (2021).
- [77] Ipsita Mandal and Emil J. Bergholtz, “Symmetry and higher-order exceptional points,” *Phys. Rev. Lett.* **127**, 186601 (2021).
- [78] Sharareh Sayyad and Flore K. Kunst, “Realizing exceptional points of any order in the presence of symmetry,” *Phys. Rev. Research* **4**, 023130 (2022).

- [79] Tsuneya Yoshida, Ryo Okugawa, and Yasuhiro Hatsugai, “Discriminant indicators with generalized inversion symmetry,” *Phys. Rev. B* **105**, 085109 (2022).
- [80] Xiaohan Cui, Ruo-Yang Zhang, Wen-Jie Chen, Zhao-Qing Zhang, and C. T. Chan, “Symmetry-protected topological exceptional chains in non-hermitian crystals,” (2022), 2204.08052.
- [81] O.N. Kirillov, “Exceptional and diabolical points in stability questions,” *Fortschritte der Physik* **61**, 205–224 (2013).
- [82] Tsuneya Yoshida and Yasuhiro Hatsugai, “Exceptional rings protected by emergent symmetry for mechanical systems,” *Phys. Rev. B* **100**, 054109 (2019).
- [83] The Supplemental Material includes details on conserved quantities in Hermitian and non-Hermitian systems and details on various phases hosted by our 2D tight-binding model.
- [84] We note that Hermitian-like nondefective degeneracies exhibit no algebraic singularities and possess stable Jordan normal form. However, the Jordan decomposition for the other nondefective degeneracies, located close to defective EPs, is unstable [44]. These subtleties in eigenvectors of two types of nondefective degeneracies should be reflected in symmetry operators ($\Upsilon_{\text{nH}}^R, \Upsilon_{\text{nH}}^L$).
- [85] The centerdot (\cdot) represents the standard composition product.
- [86] This is analog to the Wick’s rotation on the time variable from the Euclidean space into the Minkowski space.
- [87] Kohei Kawabata, Ken Shiozaki, Masahito Ueda, and Masatoshi Sato, “Symmetry and topology in non-hermitian physics,” *Phys. Rev. X* **9**, 041015 (2019).
- [88] Kohei Kawabata, Sho Higashikawa, Zongping Gong, Yuto Ashida, and Masahito Ueda, “Topological unification of time-reversal and particle-hole symmetries in non-hermitian physics,” *Nature Communications* **10** (2019).
- [89] Kai Sun, W. Vincent Liu, Andreas Hemmerich, and S. Das Sarma, “Topological semimetal in a fermionic optical lattice,” *Nature Physics* **8**, 67–70 (2011).
- [90] Shin-Ming Huang, Su-Yang Xu, Ilya Belopolski, Chi-Cheng Lee, Guoqing Chang, Tay-Rong Chang, BaoKai Wang, Nasser Alidoust, Guang Bian, Madhab Neupane, Daniel Sanchez, Hao Zheng, Horng-Tay Jeng, Arun Bansil, Titus Neupert, Hsin Lin, and M. Zahid Hasan, “New type of weyl semimetal with quadratic double weyl fermions,” *Proceedings of the National Academy of Sciences* **113**, 1180–1185 (2016).
- [91] Wei Luo, Xiaohui Wang, and Ming-Xun Deng, “A double-weyl semimetal stabilized by screw symmetry,” *Solid State Communications* **300**, 113693 (2019).
- [92] Hailong He, Chunyin Qiu, Xiangxi Cai, Meng Xiao, Manzhu Ke, Fan Zhang, and Zhengyou Liu, “Observation of quadratic weyl points and double-helical arcs,” *Nature Communications* **11** (2020).
- [93] W. B. Rui, Moritz M. Hirschmann, and Andreas P. Schnyder, “ \mathcal{PT} -symmetric non-hermitian dirac semimetals,” *Phys. Rev. B* **100**, 245116 (2019).
- [94] Jose D. H. Rivero and Li Ge, “Chiral symmetry in non-hermitian systems: Product rule and clifford algebra,” *Phys. Rev. B* **103**, 014111 (2021).
- [95] Yosuke Takasu, Tomoya Yagami, Yuto Ashida, Ryusuke Hamazaki, Yoshihito Kuno, and Yoshiro Takahashi, “PT-symmetric non-Hermitian quantum many-body system using ultracold atoms in an optical lattice with controlled dissipation,” *Progress of Theoretical and Experimental Physics* **2020** (2020), 12A110.
- [96] Anant V. Varma and Sourin Das, “Simulating many-body non-hermitian \mathcal{PT} -symmetric spin dynamics,” *Phys. Rev. B* **104**, 035153 (2021).
- [97] Roman Rausch, Robert Peters, and Tsuneya Yoshida, “Exceptional points in the one-dimensional hubbard model,” *New Journal of Physics* **23**, 013011 (2021).